R. & M. No. 3220

MINISTRY OF AVIATION

AERONAUTICAL RESEARCH COUNCIL
REPORTS AND MEMORANDA

Tests on an Experimental Three-Stage Turbine Fitted with Low Reaction Blading of Unconventional Form

By I. H. JOHNSTON and G. E. SANSOME

LONDON: HER MAJESTY'S STATIONERY OFFICE
1961
PRICE: 9*s.* 6*d.* NET

Tests on an Experimental Three-Stage Turbine Fitted with Low Reaction Blading of Unconventional Form

By I. H. JOHNSTON and G. E. SANSOME

COMMUNICATED BY THE DEPUTY CONTROLLER AIRCRAFT (RESEARCH AND DEVELOPMENT), MINISTRY OF AVIATION

*Reports and Memoranda No. 3220**

January, 1958

Summary. A three-stage turbine designed for high stage loading has been tested cold over a wide range of operating conditions and the test results have been compared with calculated performance figures.

Inter-blade row traverses have demonstrated the development of flow in a multi-stage turbine and have provided direct measurements of stator blade loss coefficients.

The relatively poor efficiency of the turbine is shown to be due to excessive losses in the rotor blade rows. It is believed that these high losses are the result of the camber-line form used in defining the profile at the root (low reaction) station.

1.0. *Introduction.* In the design of a contemporary aero-engine the task of the turbine designer is not unfortunately that of simply designing a turbine of high efficiency, but of producing a design which for the particular engine and application will give the best compromise between the rival claims of efficiency and many other factors such as size, weight and blade cooling. These all influence the geometry of the turbine stage and it is therefore necessary that the effect of each variable in the turbine stage on performance should be accurately appreciated.

The three-stage turbine was designed as a test vehicle in which some of the variables in stage design could be investigated.

The first set of blades to be tested in this turbine were of low reaction, having impulse conditions at the root, and a fairly high ratio of axial velocity to mean blade speed. The design was therefore of the type in which a relatively high work output per stage is coupled with a relatively high flow throughout. In addition the blade profiles were laid out in a systematic manner from a standard symmetrical aerofoil profile shape set around a parabolic camber-line.

This Report describes a series of tests on this blading to determine the overall performance characteristics. Comparisons are made with theoretical estimates of turbine performance based on data derived from turbine and cascade tests of conventional blading.

* Previously issued as N.G.T.E. Report No. R. 218—A.R.C. 20,179.

2.0. *Description of Test Rig.* An outline arrangement of the complete test equipment is shown in Figure 1.

Air was ducted from a supply compressor to the cubicle through a 24 in. motor controlled gate valve, a 40 in. diameter measuring section (in which was located an orifice plate with pressure tappings) and an emergency butterfly valve. The air then passed to the turbine through a combustion chamber which for these cold tests with inlet temperatures of about 100 deg C functioned merely as a length of ducting.

At exit from the turbine the air then entered a right-angled discharge duct comprising three square-sectioned cascade corners from which it diffused into a large rectangular sectioned duct. This duct was connected by a transition section to the 24 in. diameter exhaust main, from which the air was passed to the silencers.

Expansion upstream of the turbine was allowed for by incorporating a steam-type expansion joint positioned upstream of the combustion chamber, all supports from this joint to the fixed mounting at turbine outlet being free to slide. On the exhaust side various flexible bellows allowed freedom for expansion.

For power absorption, two water-cooled Heenan and Froude dynamatic brakes each having a rated maximum capacity of 3,000 h.p. at a maximum speed of 17,000 r.p.m. were available. Only one brake was used for the cold flow tests as the maximum power was only of the order of 1,000 h.p. The installation featured a form of remote torque measurement whereby torque was registered on a hydraulic weigh gear which was used in conjunction with a set of balance weights.

The field circuit for the dynamometers was from a 230 volt 50 cycle supply which is rectified before being supplied to the field and a safety circuit was incorporated whereby failure of the 230 volt supply brought in a 110 volt d.c. battery supply to maintain excitation and prevent overspeed of the turbine.

An overspeed trip device was driven by an auxiliary shaft which was coupled to the turbine *via* a worm and wheel reduction gear. This also provided a point for speed measurement.

3.0. *Description of Turbine.* 3.1. *General.* The 116 turbine was designed specifically as a research vehicle suitable for both hot and cold running and, as is shown in Figure 2, the detail construction of the unit is both unorthodox and complex. The turbine may be assembled with one, two or three stages and for each of these configurations the respective blade rows may be positioned with either a wide or narrow axial spacing. The wide spacing (0·6 in. from trailing-edge plane to leading-edge plane of the following row) was used throughout the present series of tests to facilitate traverse investigation of the air flow between blade rows.

The casing is built up from a number of aluminium-bronze half-rings which are cored out for the passage of casing cooling air. The shroud rings which form the outer annulus wall for the gas stream are located on the roots of the nozzle blades which are in turn located in the half-rings. Each of these shroud rings is made up from a number of segments joined together by spring plates and thus the ring is free to move radially with any expansion or contraction of the main casing. This feature of the design was intended to provide some variability of tip clearance during hot running, controlled by the supply of cooling air to the casing.

End thrust on the rotor assembly is taken by a Michell thrust bearing and in an attempt to obtain direct measurement of bearing torque, the bearing housing is itself mounted on roller bearings, the torque on the housing being transmitted to a statimeter. During testing this device proved to be

unsuccessful and the more orthodox method of assessing bearing power loss, namely the measurement of heat to oil, was adopted. A photograph of the assembled turbine is shown in Figure 3.

3.2. *Blade Design.* The basic design figures for the turbine blading were:

Mass flow	17·5 lb/sec
Pressure ratio $\frac{\text{outlet total}}{\text{inlet total}}$	0·34
Inlet temperature	850 deg K
Speed	10,200 r.p.m.

The velocity triangles were selected to give the following conditions at inner diameter:

Rotor blade deflection	95 deg
u_r/V_a	0·9
Impulse condition	$(\alpha_1 = -\alpha_2)$

The design triangles were then completed to conform to free-vortex flow and constant axial velocity through the turbine, the flare from turbine inlet to outlet being calculated by assuming an expansion efficiency of 90 per cent.

As all the flare occurs at the outer diameter the mean blade speed increases from Stage 1 to Stage 3. The mean stage loading based on a diameter of 14·23 in. (the mean diameter for the second stage) and defined as $2gJC_p\Delta T/u_m^2$ is equal to 3·7 where ΔT is the design stage temperature drop.

The above method of design means that at any diameter the blading for each stage is identical.

Blade profiles were constructed at two reference diameters, namely 13 in. and 17 in., and the sections at all other radii were obtained by straight-line interpolation. In contrast to 'conventional'* practice the profiles were constructed by defining a camber-line and an aerofoil. The aerofoil was a C4 section and the parabolic camber-line was selected such that the angle between chord-line and camber-line at the trailing edge was 0·3 × camber-angle.

The blade sections at the reference diameter are shown in Figures 4 and 5 and details are tabulated below:—

	Diameter	Camber	Stagger	Chord	t/c
Rotor blade	13 in.	100·7 deg	23·5 deg	1·0 in.	14
	17 in.	70 deg	36·5 deg	1·0 in.	6
Stator blade	13 in.	78·7 deg	42 deg	1·0 in.	10
	17 in.	68·6 deg	37·7 deg	1·0 in.	10

The turbine was designed with circumferential blade root fixing and therefore blade pitch can be varied by the use of suitable spacers. For the present tests 71 rotor blades and 59 stator blades were used in each stage and the variation in blade height along the turbine is shown in Figure 6.

* Actually there is no conventional system practised in the design of turbine blading, the methods varying widely between different designers. The present turbine is therefore unconventional in the sense that the blading was designed systematically to follow a particular pattern although the pattern was initially chosen in a way which might be described as intuitive or arbitrary.

4.0. *Instrumentation.* The instrumentation relevant to the aerodynamic testing of the turbine is listed below:

4.1. *Air Mass Flow.* Air flow was measured using a British Standard orifice plate of diameter 16·755 in. installed in a 40 in. diameter duct. Pressures were measured on manometers and air temperature was read by means of a Cambridge indicator and a thermocouple.

4.2. *Air Pressures.* Inlet total pressure was measured by four three-point pitot combs.

Outlet total pressure was measured by four five-point pitot combs. Each comb was equipped with a yawmeter at mean diameter and the four instruments were coupled by pinions to a circular rack which was driven by an actuator motor.

Static-pressure tappings were located at the outer annulus wall at turbine inlet, between each blade row, and at turbine outlet, and inner wall tappings were provided both upstream and downstream of the rotor.

4.3. *Air Temperatures.* Air temperature at inlet and outlet was measured by thermocouples housed in stagnation shields and observed on a potentiometer. These couples were located at three radii in the inlet annulus and at four radii in the outlet annulus. Although the temperature distribution at outlet was far from uniform, check traverses showed that a simple arithmetic mean of the four readings gave a very close approximation to the average of the detailed temperature traverse.

4.4. *Rotational Speed.* Measurement was by a Haslar tachometer driven by an extension of the turbine overspeed trip shaft and check readings were obtained from a Maxwell indicator driven by a signal from the dynamometer control generator.

4.5. *Power.* As previously mentioned, power was absorbed on a 3,000 h.p. dynamatic brake and the torque was measured on a hydraulic weigh gear. To obtain blading performance it was necessary to evaluate the bearing loss and this was assessed from measurements of oil flow and temperature rise.

The power lost to the bearings was almost all absorbed by the Michell thrust bearing and represented approximately 2 per cent of the turbine output when running cold at 7,000 r.p.m.

4.6. *Traverse Equipment.* Two remotely controlled traverse mechanisms were available and these were used to obtain pressure, flow angle and temperature traverses. Pitot yawmeters to fit these units were calibrated for measurement of total pressure, yaw angle and static pressure. Both instruments were fitted with deprector units to provide automatic yaw and the control mechanism was similar to that of the standard traverse gear[2].

At turbine inlet and after each rotor row there was provision for a radial traverse at only one circumferential point, but the sliding spacer rings of the wide build of the turbine permitted circumferential traversing behind each stator row.

5.0. *Turbine Performance.* 5.1. *Calculated Performance.* One object of this experiment was to compare measured test performance with an estimate based on the method described in Reference 1. This method requires a knowledge of the mean values for opening/pitch for each blade row and inspection figures for this are shown in Figure 7.

The calculation of turbine performance requires preliminary estimation of gas outlet angle and loss coefficient for each blade row and this information is given for reference in Tables 1 and 2. The estimated gas outlet angles and loss coefficients are shown in Figures 8 and 9.

The calculated values of efficiency and flow are not shown separately but are superimposed on the general test results and are discussed with reference to the test results in Section 5.3.

5.2. *Test Performance.* The procedure adopted for testing was to run the turbine over a wide speed range at a variety of constant pressure ratios. Efficiency was calculated from torque, speed and mass flow and also from direct measurement of temperature drop. The results of one test at constant pressure ratio are shown in Figure 10 and it will be seen that agreement between the two methods of efficiency measurement is very satisfactory. The curve shows efficiency plotted against (u_m/C) where u is the blade speed at mean diameter (14·23 in.) and C is the velocity equivalent of the isentropic heat drop per stage.

The test performance is shown in Figure 11 where efficiency and flow function are plotted against (u_m/C) for a range of pressure ratio and in Figure 12 which shows plots of the same two variables against pressure ratio for values of non-dimensional speed $(N/\sqrt{T})$.

Further testing was aimed at investigating the 'end points' of the performance map.

To obtain the runaway condition the turbine was disconnected from the brake, the only power absorption being that of the bearings. Testing covered a range of pressure ratio from 0·95 to 0·8 and the points so obtained are shown in Figure 13 related to the lowest pressure ratio test of the main programme. For these tests agreement between the two methods of power measurement was less satisfactory but the oil measurements which were preferred furnished values of efficiency repeatable to approximately $\pm$ 2 per cent which was sufficient for the purpose of the test.

The other 'end point' namely static torque was obtained by locking the rotor shaft to the dynamometer casing and measuring torque and flow for a range of pressure ratio. The flow functions thus obtained are included in Figure 11 and a general plot of torque against (u_m/C) is shown in Figure 14.

5.3. *Discussion of Results.* For a multi-stage turbine there is a unique relation between turbine flare, efficiency and pressure ratio which will satisfy the condition of constant mean axial velocity from inlet to outlet. The flare for the 116 turbine was based on a pressure ratio of 0·34 and an assumed efficiency of 90 per cent, but the curves in Figure 12 show that efficiency level is considerably lower and hence, as flare is already determined, the pressure ratio giving constant $\bar{V}a$ through the turbine must fall. Tests and calculation showed that a pressure ratio of approximately 0·37 corresponds to the condition of constant mean axial velocity.

The condition for zero incidence corresponds to a (u_m/C) of approximately 0·48 and the efficiency at a pressure ratio of 0·36 (all stages approximately matched) rises from 81 per cent to a maximum of 84 per cent at a (u_m/C) of 0·65.

It can be demonstrated that if blade loss coefficients do not vary with incidence the efficiency of any turbine stage would rise to a maximum at a stage loading $(2k_p\Delta T/u_m^2)$ of 2·0. This condition corresponds to a (u_m/C) of 0·65 for an efficiency of 84 per cent, but the calculated increase in efficiency is only approximately 1 per cent. The principal factor contributing to increase in efficiency with increase in (u_m/C) must therefore be a reduction in blade loss coefficients with negative incidence. The mean rotor incidence at (u_m/C) of 0·65 is $-$ 23 deg and therefore the inference from turbine tests is that minimum blade loss will occur at this incidence. This agrees very closely with the calculated values of blade loss coefficient over a range of incidence shown in Figure 9.

At pressure ratios below 0·37 the mean axial velocity decreases from stage to stage and the flow Reynolds number falls. The influence of the two effects is shown by the drop in efficiency from

84 per cent to 80 per cent as pressure ratio at optimum (u_m/C) is reduced from 0·36 to 0·70. In an attempt to separate the influences of Reynolds number and mismatching, the turbine performance was measured at constant pressure ratio and varying Reynolds number by throttling the exhaust.

The mean rotor Reynolds number with atmospheric exhaust was approximately $1{\cdot}5 \times 10^5$ at a turbine pressure ratio of 0·7 and an increase in Rn to $2{\cdot}5 \times 10^5$ at constant pressure ratio gave an increase in efficiency of approximately 1 per cent. With no exhaust throttle the same change in Reynolds number was equivalent to an increase in pressure ratio from 0·7 to 0·5 and an increase in efficiency of 3 per cent. It would therefore appear that the principal cause of loss in efficiency with decrease in pressure ratio is the mismatching which occurs between the stages. It should be noted that the fifth power law $(1-\eta) \propto Rn^{-1/5}$ would give a change in efficiency of approximately 1·8 per cent for the above change in Reynolds number.

An interesting feature of the characteristics of flow against (u_m/C) is that to a first order the flow is dependent only on pressure ratio from zero speed up to 45 per cent overspeed. The characteristics plotted in Figure 13 are shown merely to relate runaway conditions to the main performance, and as indicated by the broken lines they incorporate somewhat extensive extrapolation. The rise in flow function near runaway is probably accountable to 'compression' in the third and possibly the second turbine stage.

The test characteristics for the design speed $(N/\sqrt{T} = 350)$ plotted against pressure ratio in Figure 12 may be compared with the calculated performance, and at all pressure ratios the calculated efficiencies exceed test values. At the pressure ratio for maximum test efficiency the discrepancy is 2 per cent and at the matching pressure ratio (0·37) this increases to 3 per cent. It would appear that for the unconventional blading used the loss coefficients deduced from Reference 1 are optimistic, but further discussion of this question is deferred to Section 6.3.

The calculated flow characteristic for design speed is greater than the measured performance at all pressure ratios. Although the turbine flow estimate depends primarily on the values selected for gas flow angles, the calculated flow will be affected by the assumptions made regarding loss coefficients and hence efficiency. To assess this influence of efficiency, the first stage characteristic was recalculated with a rotor loss coefficient increased to provide a reduction in efficiency of 3 per cent and the flow (at constant pressure ratio) was found to decrease by approximately $1\frac{1}{2}$ per cent. Therefore although the calculated flow is 2 per cent high at low pressure ratio and $3\frac{1}{2}$ per cent high at design point, some of this discrepancy can be debited against the poor efficiency. The net error, 2 per cent at design point, is equivalent to a variation in average gas outlet angle of only 0·8 degrees.

6.0. *Traverse Results.* Preliminary investigation of the flow at turbine outlet showed that the condition of constant mean axial velocity through the turbine corresponded with a pressure ratio of approximately 0·37, and all traverses were carried out at this condition and at the non-dimensional design speed $(N/\sqrt{T} = 350)$.

6.1. *Temperature Traverses.* Temperature traverses were made at turbine inlet and at exit from each stage and the results are shown in Figure 15. The radial distribution of work in the first stage is far from constant and a measure of the non-uniformity is given by the ratio $\Delta T_{\max}/\Delta T_{\text{mean}}$, where in applying this criterion to a stage, $\Delta T_{\max}$ is taken as the temperature difference between mean inlet stage temperature and minimum outlet temperature and ΔT_{mean} is the mean stage temperature drop.

The temperature drop ratio for the first stage is 1·08 and the reduced temperature drop at each wall may be accountable partly to a reduced change of momentum due to tip clearance and partly to the retarded flows associated with the annulus wall boundary layers. These effects are more clearly shown by the velocity and angle traverses discussed in Section 6.2 and the latter data were used to compute from momentum considerations an effective radial distribution of exit temperature from the first stage. This is also shown in Figure 15, and confirms the form of the work distribution although suggesting a radial variation even larger than was obtained by temperature measurement.

The temperature profile established at exit from stage one continues through the remaining stages, but the $\Delta T_{max}/\Delta T_{mean}$ values for these stages show progressively smaller increments, this implying that there is a gradual movement towards satisfying the condition of uniform work at all blade heights.

6.2. *Traverses of Axial Velocity and Gas Angles.* The radial distributions of axial velocity and gas angles are shown in Figures 16, 17 and 18. The greatest departure from design conditions is evident in the axial velocity distributions at exit from the rotor rows where a region of low velocity is found near the inner diameter. Reference to the distribution of rotor outlet angle shows that near the inner diameter the gas angle is slightly greater than design; therefore it may be deduced that although the low axial velocity is indicative of a region of high loss, this loss is not associated with a separation of the flow from the convex surface at a point downstream of the blade passage throat. A possible explanation for such a loss may lie in the profile shape used for the rotor blade root section. Figure 5 shows that most of the turning is concentrated in the first half of the blade chord, *i.e.*, at an effective pitch/chord ratio of approximately 1·4, and therefore a flow separation upstream of the throat may be suspected. As the flow is still contained within the blade passage after the probable separation point the gas outlet angle is likely to remain unaffected, the separation being indicated only by a high loss.

The traverses of gas outlet angle show that for all blade rows the outlet angle is closely linked to the $\cos^{-1} o/s$ rule and the mean angles estimated in the performance calculation give good agreement with the measured angles. All rotor blade rows are shown to be at negative incidence, and this is because the overall turbine pressure ratio was reduced from the design value to provide a condition of constant mean axial velocity through the three stages.

6.3. *Loss Traverses.* Circumferential traverses for total pressure loss were made over a blade pitch and for a range of blade height behind each stator row.

The radial variations of loss expressed as a percentage of the mean exit dynamic head are shown in Figure 19. The distribution of loss for the first stator row is of conventional form. The low loss at mean diameter which is related to the profile loss and the end losses due to secondary flows and tip clearance effects are clearly defined. The average loss coefficient is 0·115 as compared with an estimated loss coefficient of 0·105.

The first stator row is receiving a uniform axial flow and is thus operating at − 12 deg incidence whereas the second and third stator rows receive a very non-uniform flow at substantially zero incidence (*see* Figures 17 and 18). The loss traverses for these rows are notable for the unexpectedly high level of loss at mean diameter which cannot be explained in terms of excessive incidence and must therefore be related to the very non-uniform flows which enter the blading from the preceding rotor rows.

An average value for measured stator loss coefficient is 0·120 compared with an average estimated value of 0·113 and at traverse pressure ratio (0·37) and speed ($N/\sqrt{T} = 350$) this change in stator loss is equivalent to a change in efficiency of $\frac{1}{2}$ per cent. There is a total discrepancy in efficiency of 3 per cent, therefore $2\frac{1}{2}$ per cent is accountable to the rotor rows, and this corresponds to an increase in average rotor loss coefficient from 0·2 to 0·26. This marked increase in rotor loss coefficient is further evidence of the unsuitability of the rotor blade form previously commented on in Section 6.2.

Note. The values of measured total loss coefficient must be treated with some reserve as it was not found possible to achieve 'cascade tunnel' accuracy when traversing in the turbine, primarily because of mechanical considerations which limited the range of the traverse near the outer wall.

7.0. *Effect of Tip Clearance.* In practice most modern turbine designs would incorporate some form of tip sealing for at least the stator blade rows and the performance of the somewhat unconventional blade profiles of the design tested is rather unfairly prejudiced by the radial clearance on all blade rows.

The estimated effect of this clearance is that it contributes a loss of 0·05 to the total loss coefficient of the row and if we assume that this loss could be entirely eliminated for each stator row by some form of efficient shroud it can be estimated that the efficiency at a turbine pressure ratio of 0·37 and at design speed would increase from 82 to 85 per cent.

8.0. *Conclusions.* 1. A three-stage turbine designed for a pressure ratio ($\frac{\text{outlet total pressure}}{\text{inlet total pressure}}$) of 0·34 and a speed ($N/\sqrt{T}$) of 350 has been tested and is found to have an efficiency at design point of 82 per cent.

2. An estimate of efficiency calculated by the method of Reference 1 is 3 per cent higher than the measured efficiency at design point.

3. The calculated flow is $3\frac{1}{2}$ per cent above measured flow at design pressure ratio, the discrepancy reducing to 2 per cent at low pressure ratio.

4. The average measured stator total loss coefficient is 7 per cent in excess of the estimated value. As this is equivalent to a difference in efficiency of only 0·5 per cent the method of stator loss estimation would appear to be satisfactory.

5. The low level of efficiency is due mainly to the high average rotor loss coefficient which exceeds the estimate by approximately 30 per cent. The cause of this high loss is thought to be the unconventional blade section used near the root of the rotor.

6. Whilst there may be a benefit to be obtained from a more rational and systematic method for defining turbine blade profile shape than exists at present it is clear that the 'systematic', but unconventional, procedure adopted in the present design is not to be recommended. It seems probable that a more 'conventional' impulse profile in the vicinity of the blade root, with curvature distributed more evenly over the blade chord, would give an improved efficiency.

7. It is estimated that the efficiency of the turbine would rise from 82 per cent to 85 per cent if nozzle tip clearance effects could be completely eliminated.

Acknowledgements. The authors are indebted to Messrs. L. R. Knight and N. E. Waldren for their valuable assistance in the installation and operation of the test equipment and to Mr. J. Pollock who performed a large part of the computation.

NOTATION

α	Gas inlet angle
α_2	Gas outlet angle
α_m	Vector mean gas angle
β_1	Blade inlet angle
c	Blade chord
C_L	Lift coefficient based on vector mean velocity
e	Mean radius of curvature of upper surface between throat and trailing edge
s	Blade pitch
K	Tip clearance
h	Blade height
A_N	Annulus area
A_t	Throat area
λ	A factor defining secondary loss
B	A constant affecting clearance loss
o	Blade opening
W	Mass flow
T	Temperature
P	Pressure
Y_p	Profile loss coefficient
Y_s	Secondary loss coefficient
Y_k	Clearance loss coefficient
Y_t	Total loss coefficient
η	Isentropic efficiency
u_m	Blade speed at mean diameter
u_r	Blade speed at inner diameter
C	Velocity equivalent of isentropic heat drop per stage
C_p	Specific heat

An accented alpha, α', denotes gas angle not corrected for tip clearance

---

REFERENCES

No.	*Authors*	*Title, etc.*
1	D. G. Ainley and G. C. R. Mathieson	A method of performance estimation for axial flow turbines. R. & M. 2974. December, 1951.
2	H. Shaw and H. Ogden	The application of remote control and indication to a high speed cascade tunnel. A.R.C. 13,664. October, 1950.

TABLE 1

Calculation of Gas Outlet Angles (using Method of Reference 1)

	Stator 1	Rotor 1	Stator 2	Rotor 2	Stator 3	Rotor 3
Zero tip clearance						
	$M_n \leqslant 0{\cdot}5$					
Reference diameter .	13·945	13·945	14·234	14·234	14·753	14·753
o/s . . .	0·494	0·54	0·488	0·559	0·508	0·545
s	0·744	0·617	0·76	0·63	0·785	0·654
e	1·59	1·86	1·59	1·85	1·59	1·84
s/e . . .	0·47	0·33	0·48	0·34	0·49	0·36
$\alpha_2{}^*$ . . .	−58·2	−54·6	−58·7	−53·3	−57·2	−54·4
$\alpha_2{}'$ . . .	−60·07	−55·93	−60·61	−54·66	−59·18	−55·82
	$M_n = 1{\cdot}0$					
A_{N1} . . .	62·1	62·1	66·94	77·34	88·8	104·2
A_{N2} . . .	62·1	66·94	77·34	88·8	104·2	121·0
$A_t{}'$ . . .	30·65	35·71	38·89	48·57	51·58	64·42
$\alpha_2{}'$ . . .	−60·43	−57·77	−61·50	−56·85	−60·33	−57·83
Angles corrected for radial tip clearance						
	$M_n \leqslant 0{\cdot}5$					
$\tan\alpha'_2$ . . .	−1·737	−1·479	−1·776	−1·41	−1·676	−1·473
$\cos\alpha'_2$ . . .	−0·499	−0·56	−0·49	−0·579	−0·512	−0·562
β_1	12·4	38·8	12·3	36·4	12·0	32·0
$\cos\beta_1$ . . .	0·977	0·779	0·977	0·805	0·978	0·848
$\tan\beta_1$ . . .	0.219	0·804	0·218	0·737	0·213	0·625
X			1·35			
K	0·036	0·036	0·035	0·051	0·042	0·062
h	1·42	1·52	1·73	1·955	2·25	2·558
α_2	−58·56	−55·38	−59·4	−54·02	−58·08	−55·05
	$M_N = 1{\cdot}0$					
A'_t . . .	30·65	35·71	36·89	48·57	51·58	64·42
A_t . . .	31·60	36.61	37.88	49.96	52.82	66.22
α_2	−59·4	−56·85	−60·65	−55·8	−59·53	−56·82

TABLE 2

Calculation of Loss Coefficients at Zero Incidence

Profile loss at zero incidence

	Stator 1	Rotor 1	Stator 2	Rotor 2	Stator 3	Rotor 3
β_1	12·4	38·8	12·3	36·4	12·0	32·0
α_2'	−60·07	−55·93	−60·6	−54·66	−59·18	−55·82
s/c	0·744	0·617	0·76	0·63	0·785	0·654
β_1/α_2'	−0·204	−0·694	−0·203	−0·666	−0·203	−0·574
t/c	0.10	0.10	0.10	0.10	0.10	0.10
Y_p $(\beta_1 = 0)$	0·026	0·032	0·026	0·031	0·025	0·029
Y_p $(\beta_1 = -\alpha_2')$	0.105	0.089	0.108	0.086	0.104	0·089
Y_p	0·025	0·037	0·025	0·035	0·025	0·033

Secondary and clearance losses at zero incidence

K	0·036	0·036	0·035	0·051	0·042	0·062
h	1·42	1·47	1·625	1·843	2·103	2·404
K/h	0·025	0·025	0·022	0·028	0·02	0·026
$\alpha_1' - \alpha_2'$	72·47	94·73	72·9	91·06	71·18	87·82
$C_L/(s/c)$	3·125	4·325	3·145	4·07	3·055	3·86
$\cos^2\alpha_2'/\cos^3\alpha_m$	0·494	0·370	0·491	0·394	0·500	0·405
A_1	60·65	48·39	65·4	62·25	86·86	88·36
A_2	30·99	37·49	37·97	51·36	53·38	67·97
A_2/A_1	0·511	0·775	0·580	0·825	0·615	0·769
ID/OD	0·815	0·810	0·795	0·773	0·749	0·721
λ	0.007	0.015	0.008	0.019	0.009	0·016
B	0·5	0·5	0·5	0·5	0·5	0·5
Y_s	0·034	0·102	0·040	0·123	0·042	0·094
Y_k	0·060	0·087	0·053	0·091	0·047	0·078
$Y_s + Y_k$	0·094	0·188	0·094	0·214	0·089	0·0172

Total loss coefficient at zero incidence

Y_t $(t_e/s = 0·02)$	0·120	0·225	0·118	0·249	0·114	0·205
Y_t $(t_e/s$ actual$)$	0·118	0·23	0·117	0·261	0·114	0·204

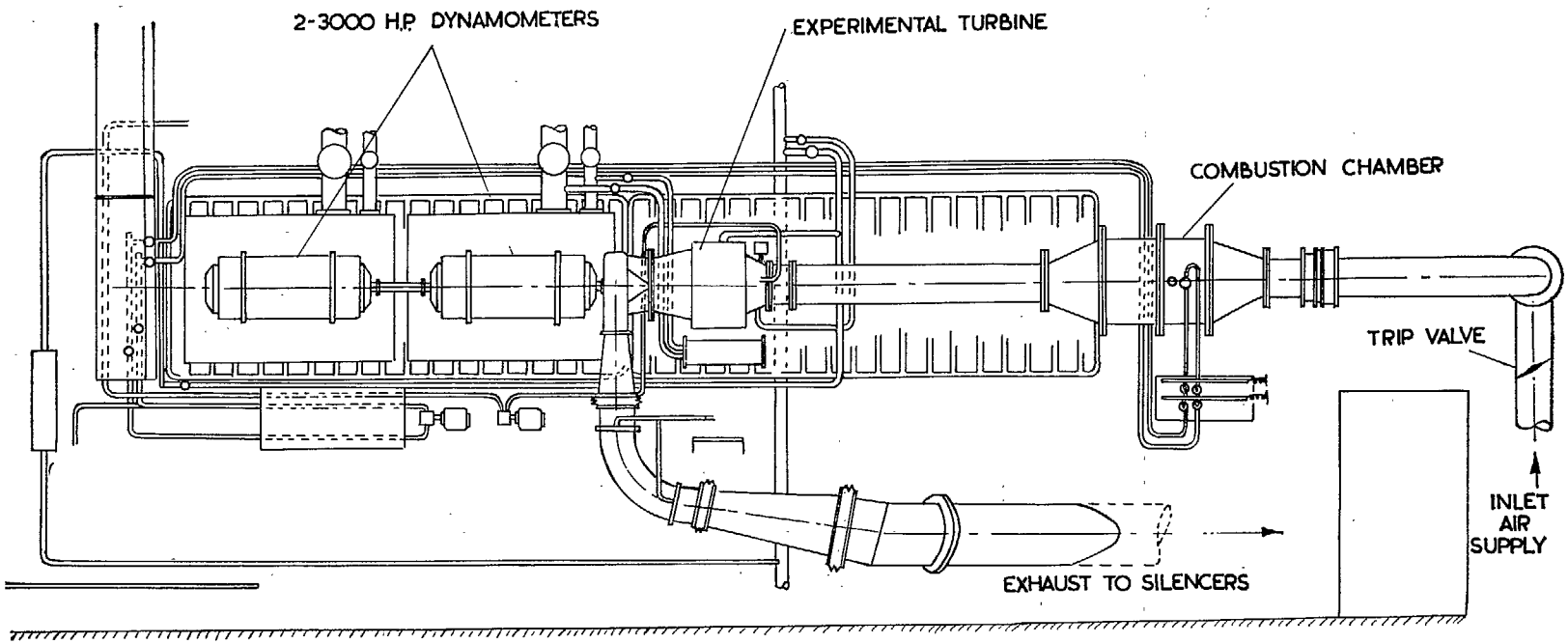

FIG. 1. Layout of test equipment.

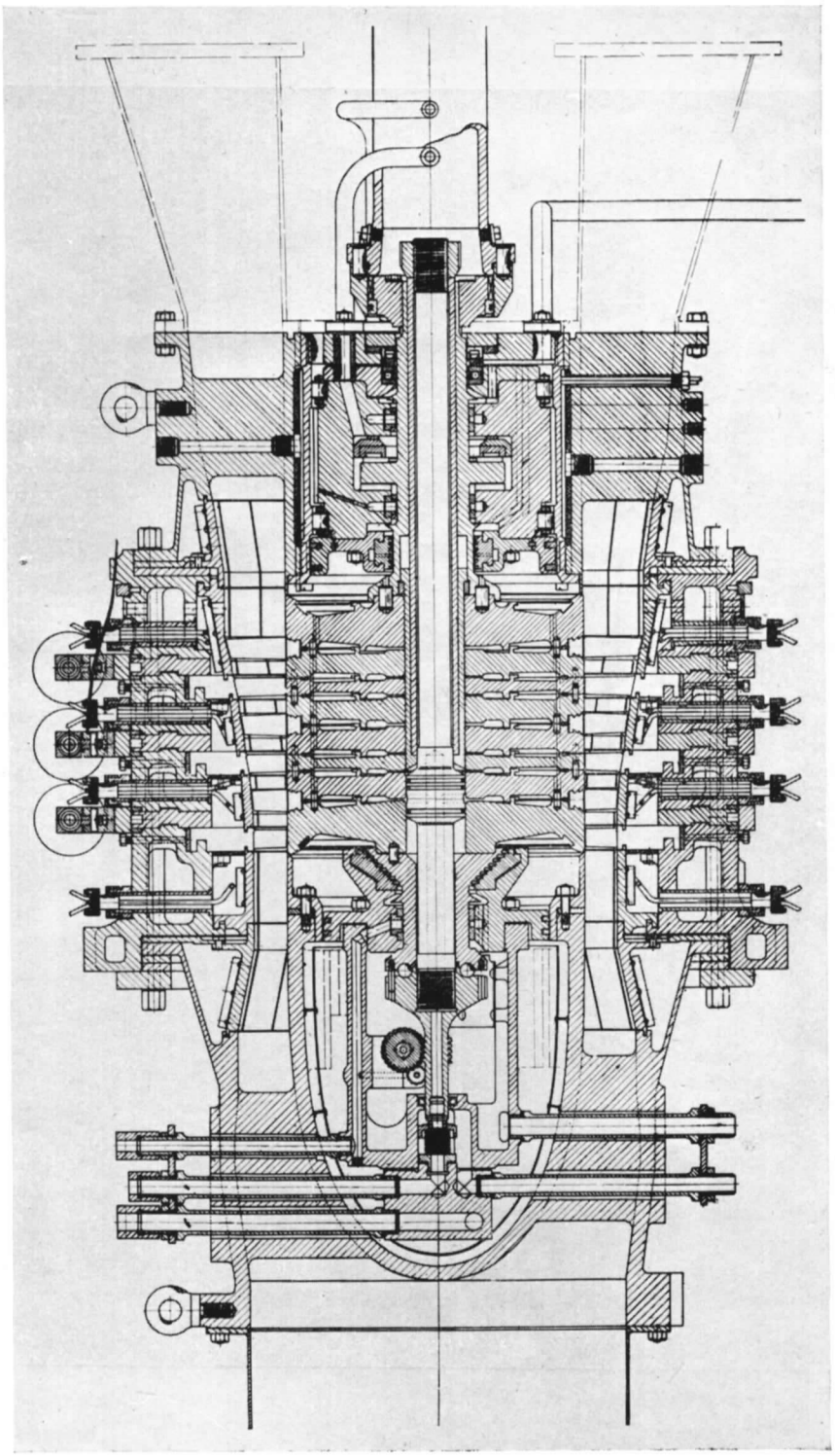

FIG. 2. Section of turbine.

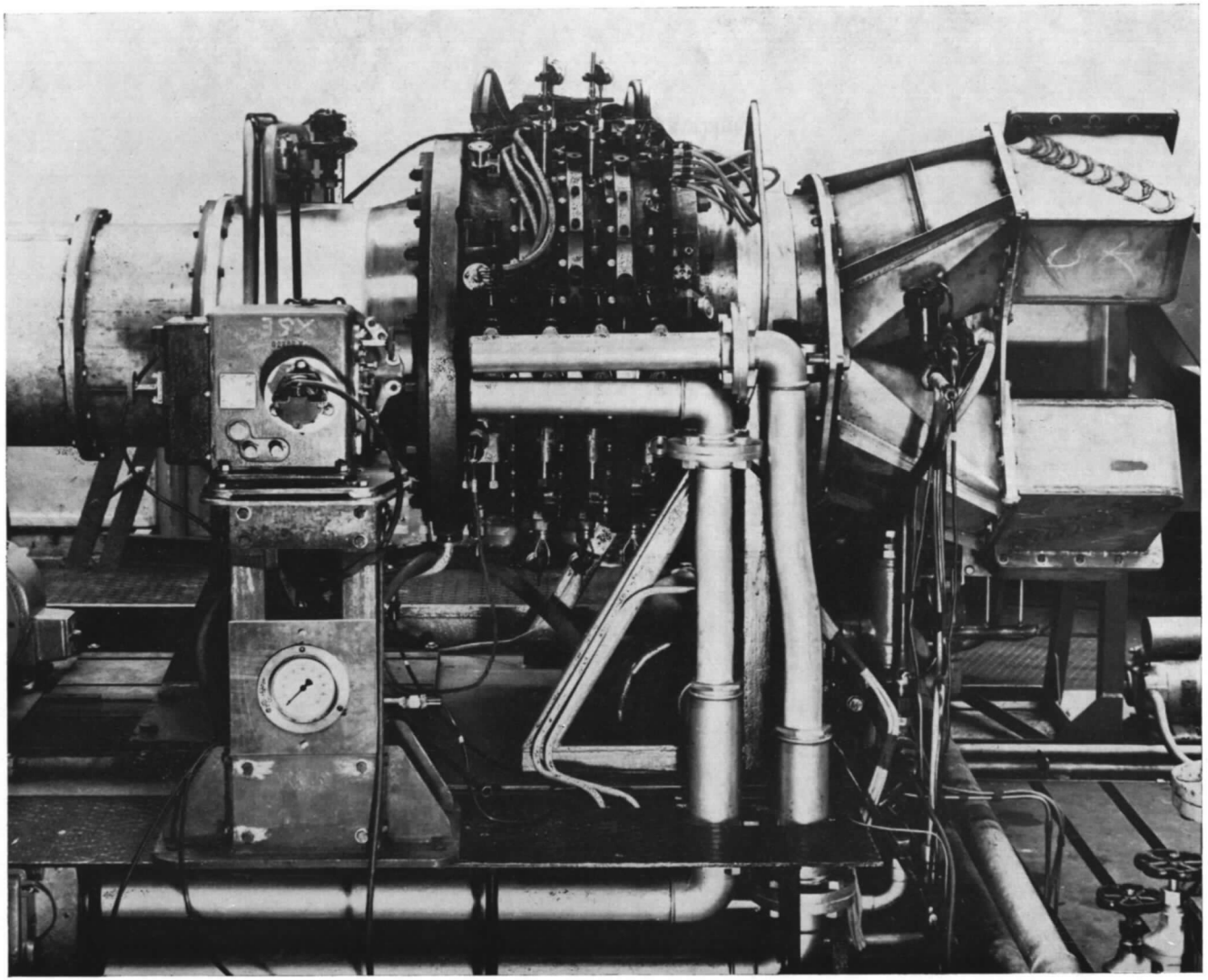

FIG. 3. Photograph of turbine.

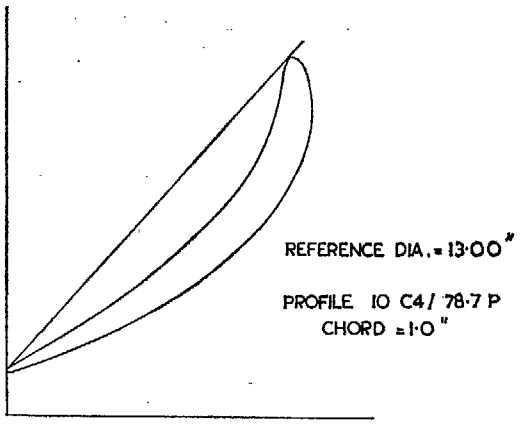

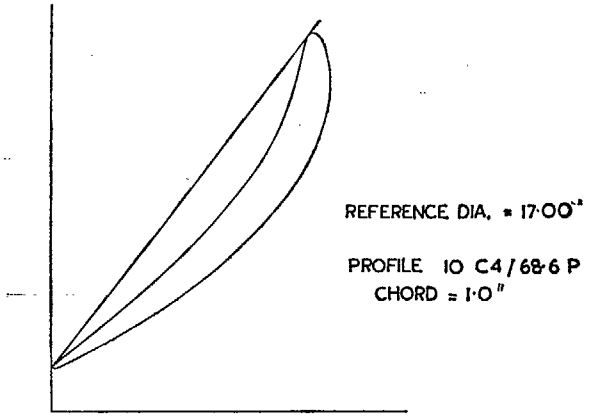

FIG. 4. Stator blade profiles.

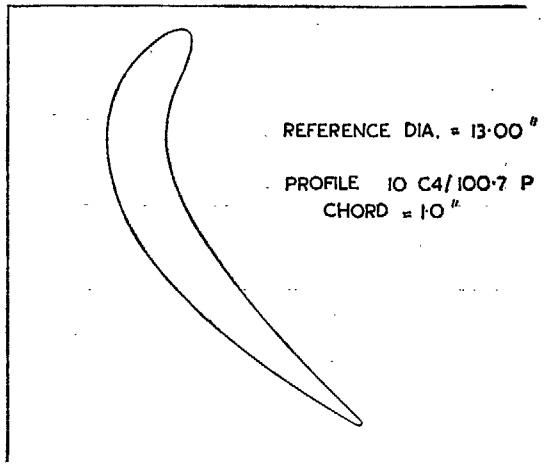

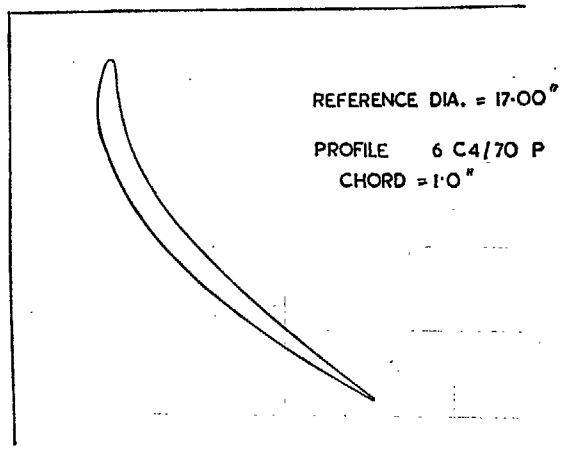

FIG. 5. Rotor blade profiles.

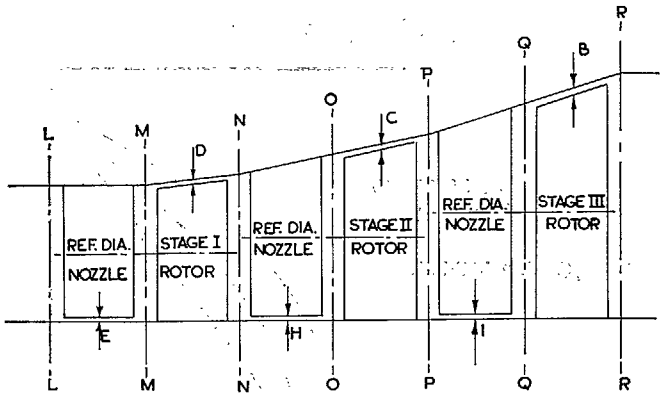

FROM RUSTON & HORNSBY DRAWINGS			
STATION	ANNULUS O.D.	ANNULUS I.D.	ANNULUS AREA
LL	15·34	12·5	62·1 A_{N1}
MM	15·34	12·5	62·1 A_{No} $A_{N1(1)}$
NN	15·54	12·5	66·94 A_{N2} $A_{N3(2)}$
OO	15·96	12·5	77·34 $A_{No(2)}$ $A_{N1(2)}$
PP	16·41	12·5	88·8 $A_{N2(2)}$ $A_{N3(3)}$
QQ	17·00	12·5	104·2 $A_{No(3)}$ $A_{N1(3)}$
RR	17·6156	12·5	121·0 $A_{N2(3)}$

	STAGE I	STAGE II	STAGE III
REFERENCE DIAMETER	13·945	14·23375	14·7532

STATION	E	D	H	C	I	B
TIP CLEARANCE-K INSPECTION VALUES	0·036	0·036	0·035	0·051	0·042	0·062

FIG. 6. Three-stage turbine dimensions.

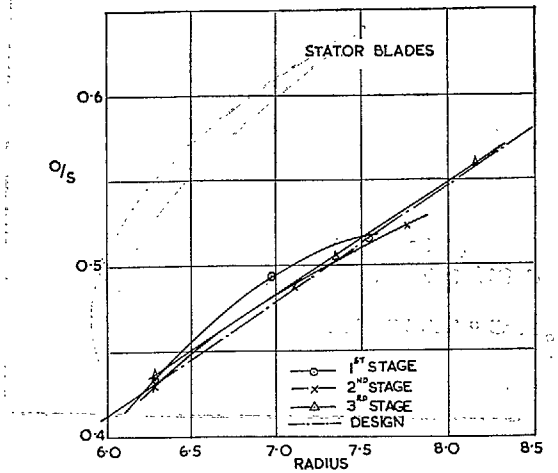

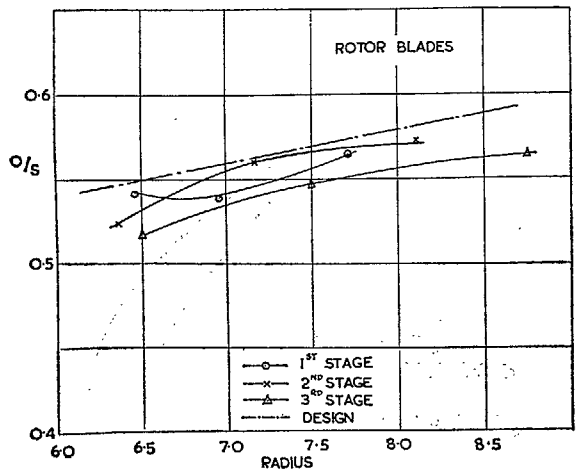

FIG. 7. Three-stage turbine $\frac{\text{throat}}{\text{pitch}}$ inspection figures.

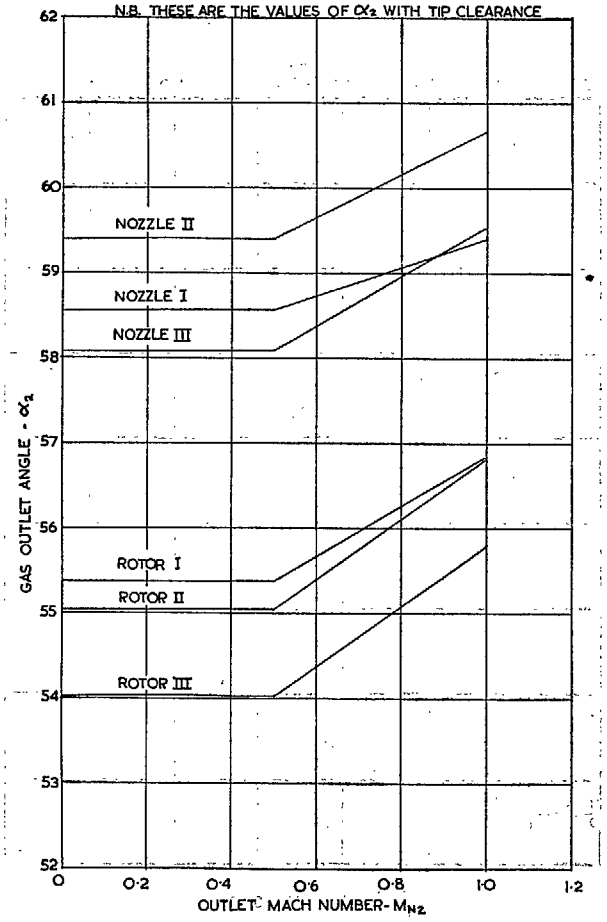

FIG. 8. Estimated gas outlet angles.

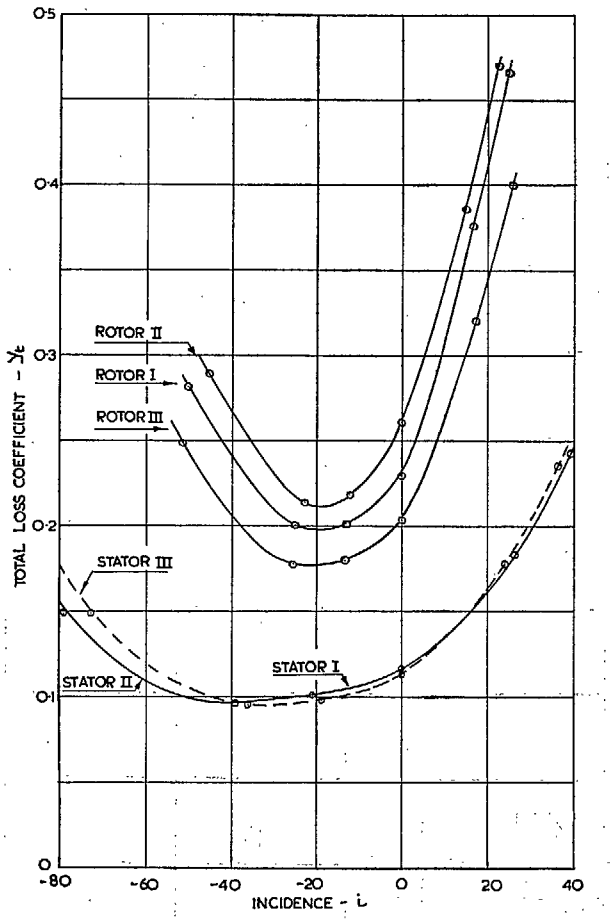

FIG. 9. Estimated total loss coefficients.

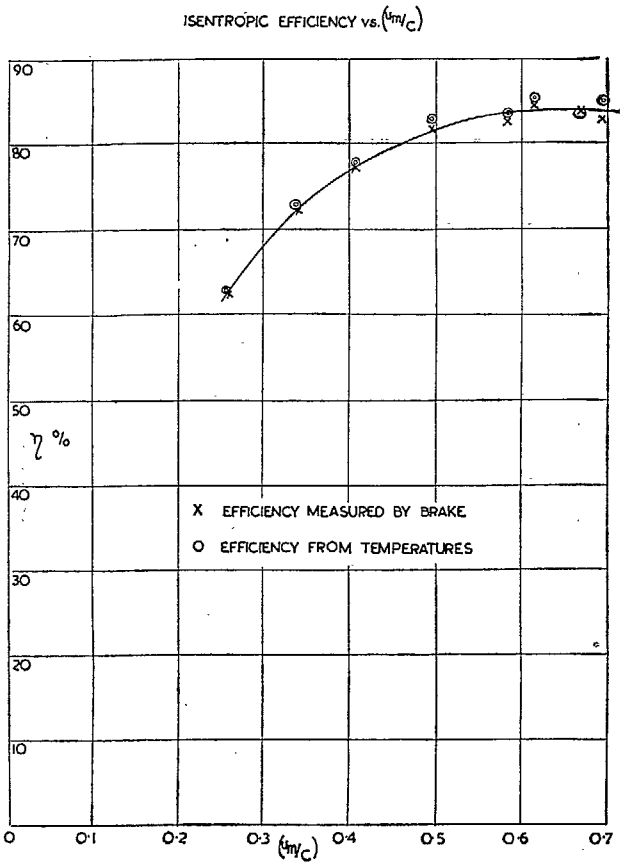

FIG. 10. Comparison between 'brake' and 'temperature' measurements.

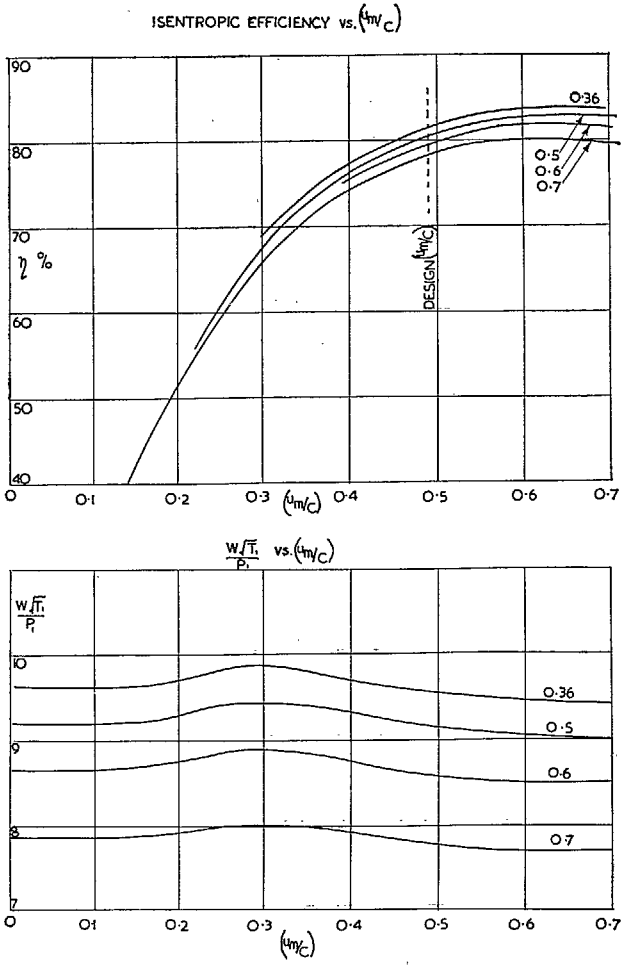

FIG. 11. Turbine test results (total pressure ratios shown on curves).

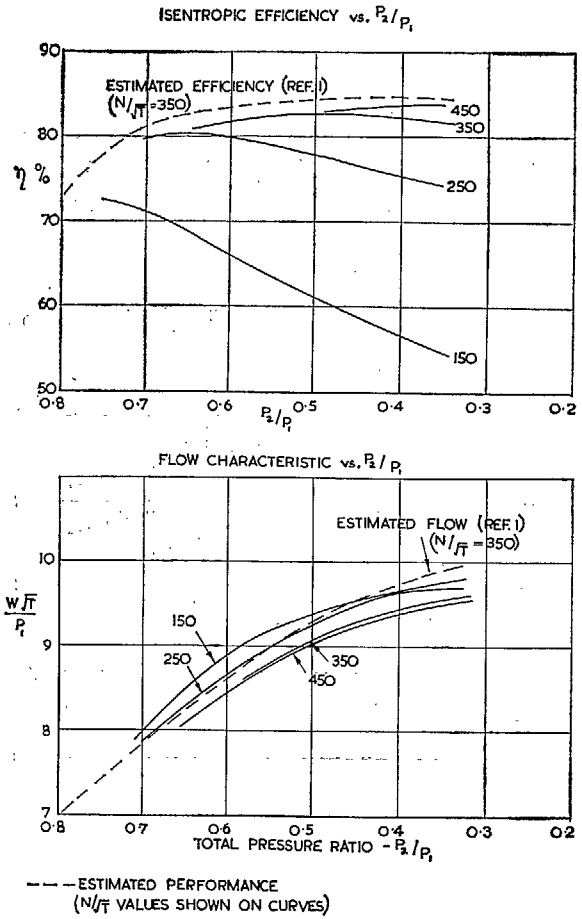

FIG. 12. Turbine test results.

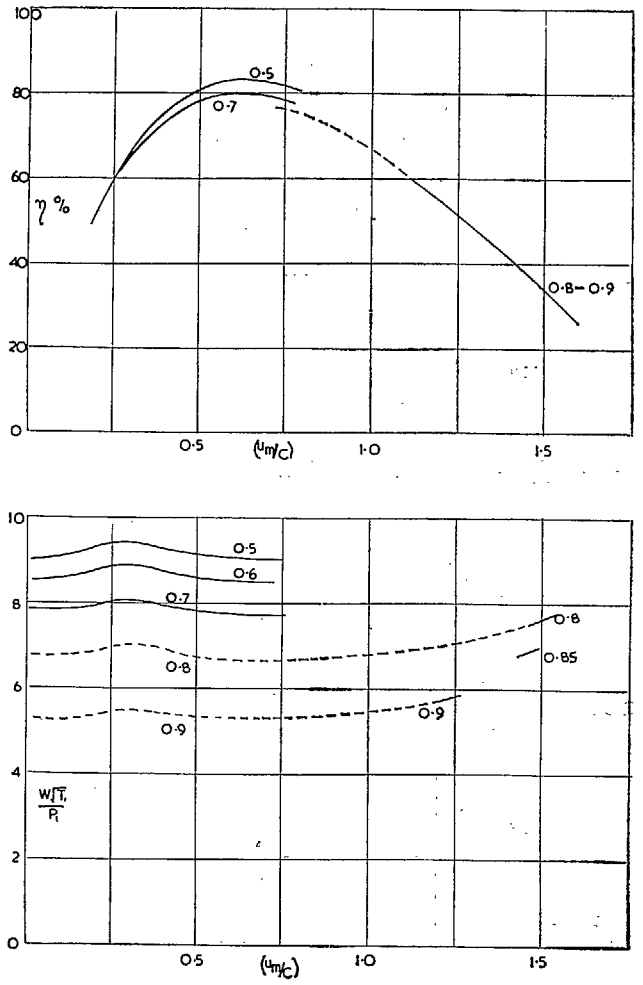

FIG. 13. Test results showing runaway conditions (pressure ratios shown on curves).

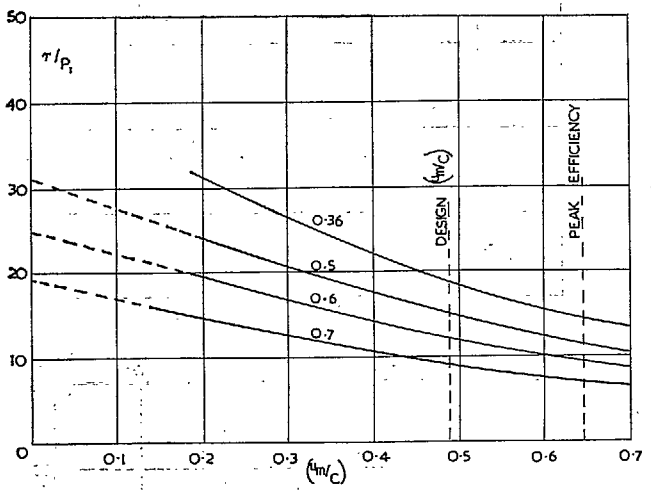

FIG. 14. Torque characteristic for 3-stage turbine.

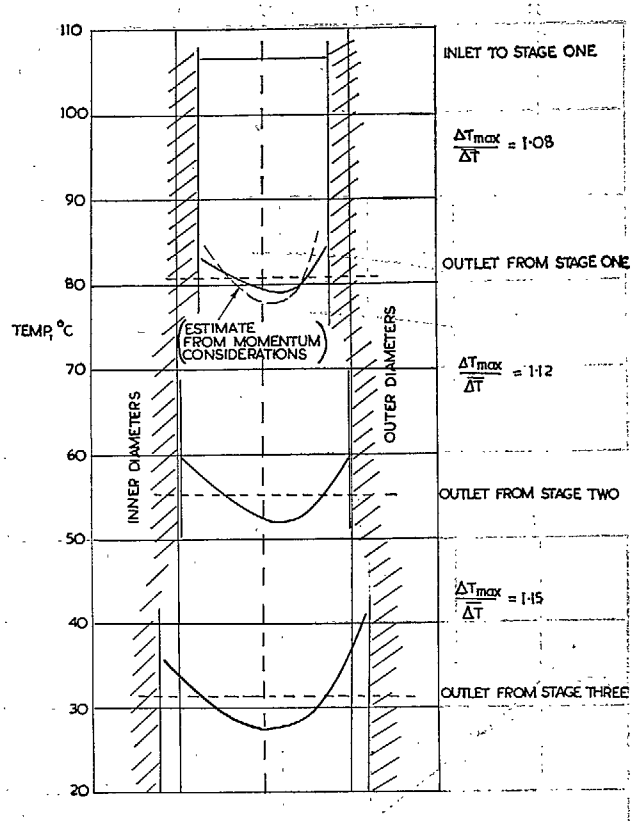

FIG. 15. Temperature traverses (running conditions approximately $P_2/P_1 = 0{\cdot}375$, $N/\sqrt{T} = 350$).

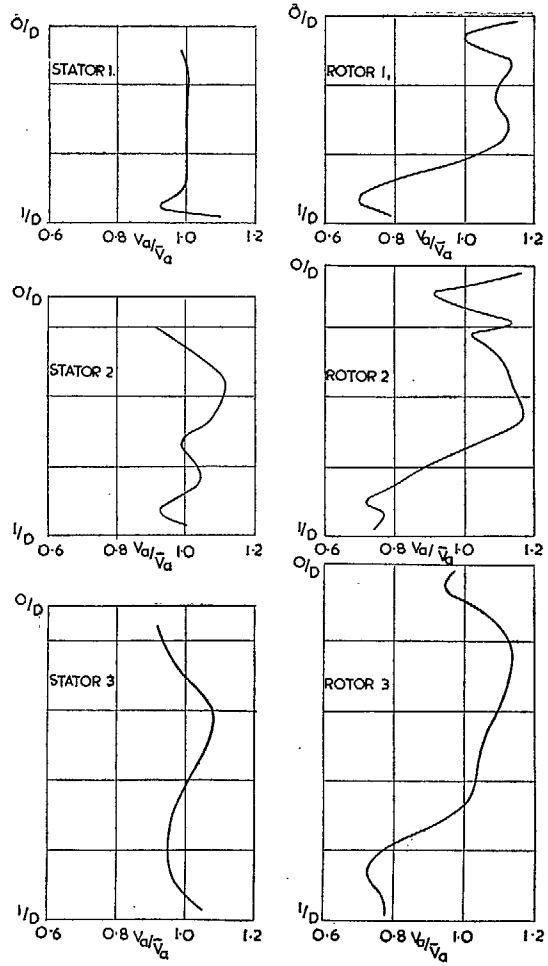

FIG. 16. Axial velocity profiles at exit from each blade row.

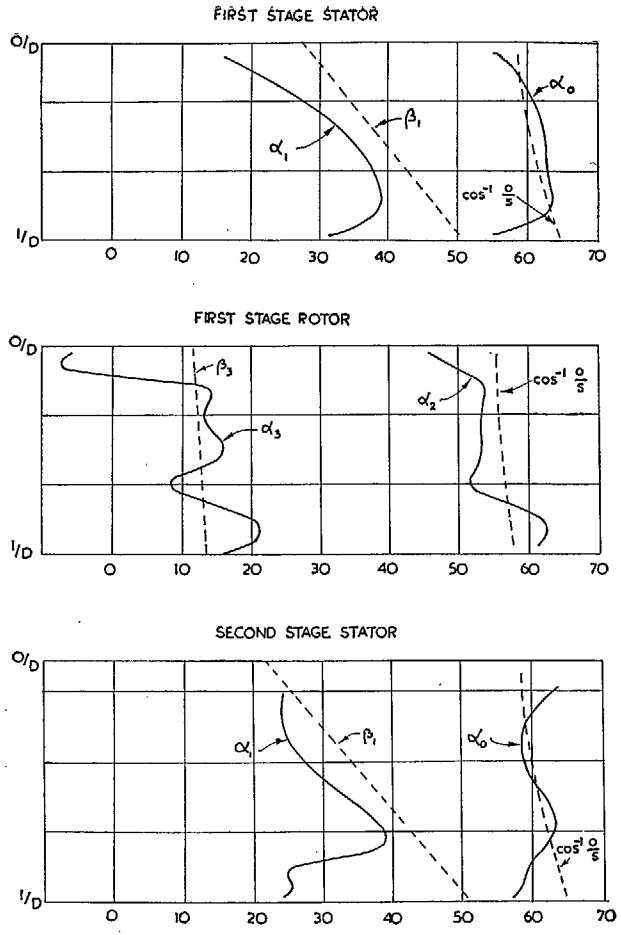

FIG. 17. Flow angles at exit from first stator, first rotor and second stator (– – – – $\cos^{-1}\frac{\text{opening}}{\text{pitch}}$).

(82479) Wt. 66/991 K.5 9/61 Hw.

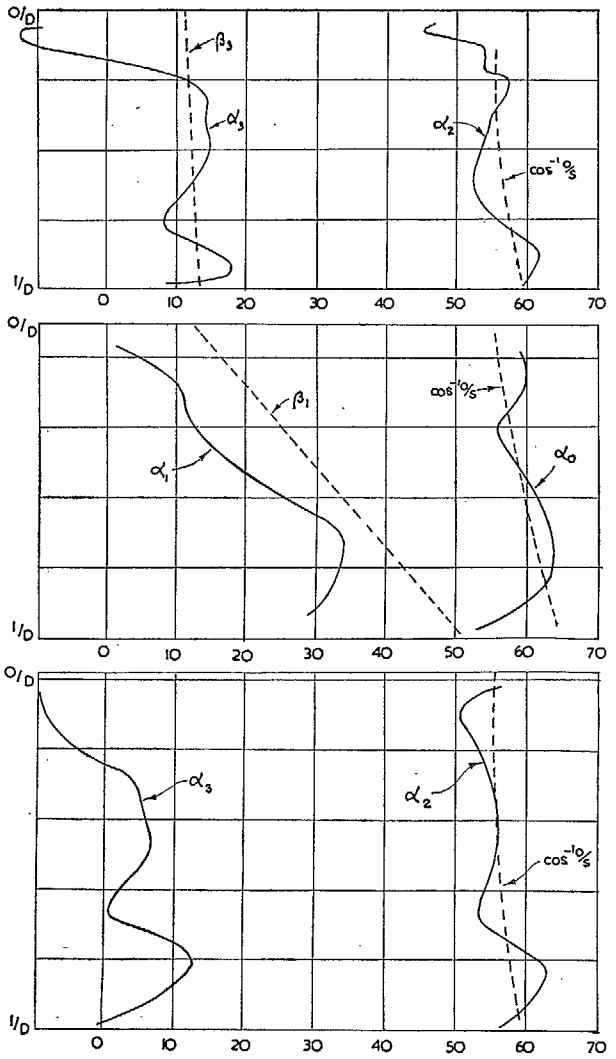

FIG. 18. Flow angles at exit from second rotor, third stator and third rotor.

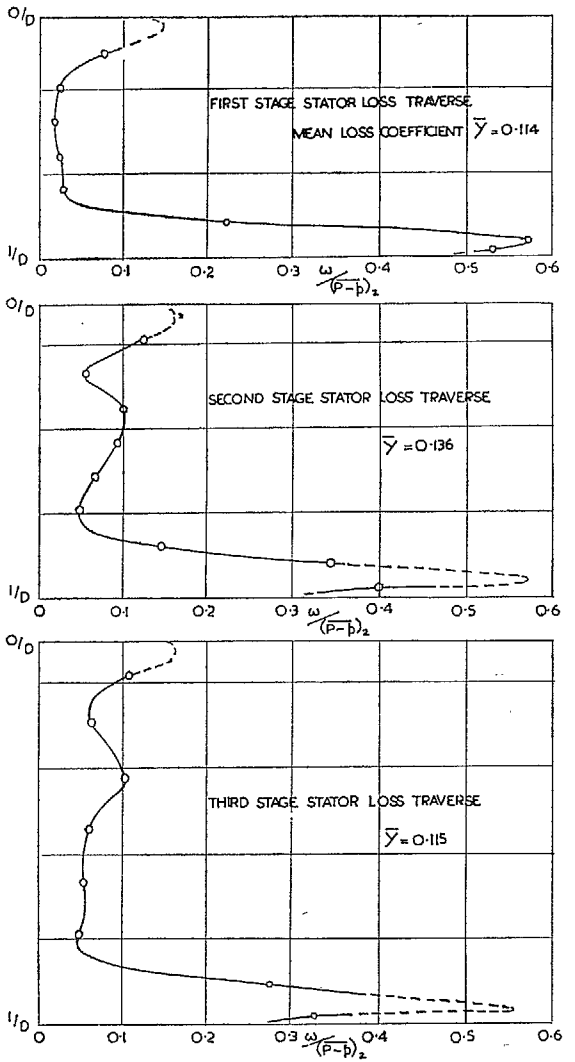

FIG. 19. Loss traverses.

Publications of the Aeronautical Research Council

ANNUAL TECHNICAL REPORTS OF THE AERONAUTICAL RESEARCH COUNCIL (BOUND VOLUMES)

1941 Aero and Hydrodynamics, Aerofoils, Airscrews, Engines, Flutter, Stability and Control, Structures. 63*s.* (post 2*s.* 3*d.*)

1942 Vol. I. Aero and Hydrodynamics, Aerofoils, Airscrews, Engines. 75*s.* (post 2*s.* 3*d.*)
Vol. II. Noise, Parachutes, Stability and Control, Structures, Vibration, Wind Tunnels. 47*s.* 6*d.* (post 1*s.* 9*d.*)

1943 Vol. I. Aerodynamics, Aerofoils, Airscrews. 80*s.* (post 2*s.*)
Vol. II. Engines, Flutter, Materials, Parachutes, Performance, Stability and Control, Structures. 90*s.* (post 2*s.* 3*d.*)

1944 Vol. I. Aero and Hydrodynamics, Aerofoils, Aircraft, Airscrews, Controls. 84*s.* (post 2*s.* 6*d.*)
Vol. II. Flutter and Vibration, Materials, Miscellaneous, Navigation, Parachutes, Performance, Plates and Panels, Stability, Structures, Test Equipment, Wind Tunnels. 84*s.* (post 2*s.* 6*d.*)

1945 Vol. I. Aero and Hydrodynamics, Aerofoils. 130*s.* (post 3*s.*)
Vol. II. Aircraft, Airscrews, Controls. 130*s.* (post 3*s.*)
Vol. III. Flutter and Vibration, Instruments, Miscellaneous, Parachutes, Plates and Panels, Propulsion. 130*s.* (post 2*s.* 9*d.*)
Vol. IV. Stability, Structures, Wind Tunnels, Wind Tunnel Technique. 130*s.* (post 2*s.* 9*d.*)

1946 Vol. I. Accidents, Aerodynamics, Aerofoils and Hydrofoils. 168*s.* (post 3*s.* 3*d.*)
Vol. II. Airscrews, Cabin Cooling, Chemical Hazards, Controls, Flames, Flutter, Helicopters, Instruments and Instrumentation, Interference, Jets, Miscellaneous, Parachutes. 168*s.* (post 2*s.* 9*d.*)
Vol. III. Performance, Propulsion, Seaplanes, Stability, Structures, Wind Tunnels. 168*s.* (post 3*s.*)

1947 Vol. I. Aerodynamics, Aerofoils, Aircraft. 168*s.* (post 3*s.* 3*d.*)
Vol. II. Airscrews and Rotors, Controls, Flutter, Materials, Miscellaneous, Parachutes, Propulsion, Seaplanes, Stability, Structures, Take-off and Landing. 168*s.* (post 3*s.* 3*d.*)

Special Volumes

Vol. I. Aero and Hydrodynamics, Aerofoils, Controls, Flutter, Kites, Parachutes, Performance, Propulsion, Stability. 126*s.* (post 2*s.* 6*d.*)
Vol. II. Aero and Hydrodynamics, Aerofoils, Airscrews, Controls, Flutter, Materials, Miscellaneous, Parachutes, Propulsion, Stability, Structures. 147*s.* (post 2*s.* 6*d.*)
Vol. III. Aero and Hydrodynamics, Aerofoils, Airscrews, Controls, Flutter, Kites, Miscellaneous, Parachutes, Propulsion, Seaplanes, Stability, Structures, Test Equipment. 189*s.* (post 3*s.* 3*d.*)

Reviews of the Aeronautical Research Council

1939–48 3*s.* (post 5*d.*) 1949–54 5*s.* (post 5*d.*)

Index to all Reports and Memoranda published in the Annual Technical Reports

1909–1947 R. & M. 2600 6*s.* (post 2*d.*)

Indexes to the Reports and Memoranda of the Aeronautical Research Council

Between Nos. 2351–2449	R. & M. No. 2450	2*s.* (post 2*d.*)
Between Nos. 2451–2549	R. & M. No. 2550	2*s.* 6*d.* (post 2*d.*)
Between Nos. 2551–2649	R. & M. No. 2650	2*s.* 6*d.* (post 2*d.*)
Between Nos. 2651–2749	R. & M. No. 2750	2*s.* 6*d.* (post 2*d.*)
Between Nos. 2751–2849	R. & M. No. 2850	2*s.* 6*d.* (post 2*d.*)
Between Nos. 2851–2949	R. & M. No. 2950	3*s.* (post 2*d.*)
Between Nos. 2951–3049	R. & M. No. 3050	3*s.* 6*d.* (post 2*d.*)

HER MAJESTY'S STATIONERY OFFICE

from the addresses overleaf

Printed and published by
HER MAJESTY'S STATIONERY OFFICE

To be purchased from
York House, Kingsway, London W.C.2
423 Oxford Street, London W.1
13A Castle Street, Edinburgh 2
109 St. Mary Street, Cardiff
39 King Street, Manchester 2
50 Fairfax Street, Bristol 1
2 Edmund Street, Birmingham 3
80 Chichester Street, Belfast 1
or through any bookseller

Printed in England

S.O. Code No. 23-3220